Nucleon spectral function at finite temperature and the onset of superfluidity in nuclear matter

T. Alm, G. Röpke, and A. Schnell
Arbeitsgruppe der Max-Planck-Gesellschaft ''Theoretische Vielteilchenphysik'' an der Universität, Rostock, Universitätsplatz 1, D-18051 Rostock, Germany

N. H. Kwong and H. S. Köhler
Physics Department, University of Arizona, Tuscon, Arizona 85721
(Received 27 November 1995)

Nucleon self-energies and spectral functions are calculated at the saturation density of symmetric nuclear matter at finite temperatures. In particular, the behavior of these quantities at temperatures above and close to the critical temperature for the superfluid phase transition in nuclear matter is discussed. It is shown how the singularity in the thermodynamic T matrix at the critical temperature for superfluidity (Thouless criterion) reflects in the self-energy and correspondingly in the spectral function. The real part of the on-shell self-energy (optical potential) shows an anomalous behavior for momenta near the Fermi momentum and temperatures close to the critical temperature related to the pairing singularity in the imaginary part. For comparison the self-energy derived from the K matrix of Brueckner theory is also calculated. It is found that there is no pairing singularity in the imaginary part of the self-energy in this case, which is due to the neglect of hole-hole scattering in the K matrix. From the self-energy the spectral function and the occupation numbers for finite temperatures are calculated. [S0556-2813(96)02305-9]

PACS number(s): 21.65.+f, 21.10.Pc, 21.30.Fe

I. INTRODUCTION

Heavy-ion reactions at intermediate energies probe the nuclear equation of state in a broad temperature and density range. One tries to extract from the observables signals for cluster formation, multifragmentation or the liquid-gas phase transition. The theoretical description of such phenomena demands to go beyond the usual quasiparticle description for the equilibrium properties [equation of state (EOS)] as well as for the nonequilibrium properties (Boltzmann-Uehling-Uhlenback simulations). The need to go beyond the quasiparticle approximation in the description of nuclear matter is further advocated by the electron-scattering experiments from heavy nuclei. These experiments give a clear evidence that the one-nucleon spectral function shows pronounced deviations from mean-field estimates, which are due to nucleon-nucleon (NN) correlations [1]. The effect of these correlations can most accurately be studied for nuclear matter [2].

A systematic quantum statistical approach for the description of dense nuclear matter can be given using Green-function theory. For the description of phenomena like the formation of clusters (bound states) in the medium or the onset of a superfluid phase, one has to allow for a finite lifetime (damping) of the one particle states. Such a treatment can be based on the nucleon spectral function, which is defined in terms of the real and imaginary parts of the self-energy. Having the nucleon spectral function at the disposal, one is able to determine the momentum distribution, the response function as well as the nuclear equation of state including correlations beyond the mean-field level.

Most of the existing calculations of the nucleon spectral function have been done for zero temperature nuclear matter at the saturation density n_0. In Refs. [3–5] it is shown that the quasiparticle description is only valid near the Fermi energy. In general, the spectral function has a considerable width indicating that the one-particle states are strongly damped at the saturation density. Baldo *et al.* [3] calculated the on- and off-shell properties of the nucleon mass operator and the nucleon spectral function. They stressed the importance to retain the full frequency dependence of the self-energy for the calculation of the spectral function. Köhler [4] compared the nucleon spectral function calculated within Green-function theory with a calculation done in Brueckner theory. He pointed out the near equivalence between the two theories at zero temperature. Vonderfecht *et al.* [5] used Green-function theory to calculate the nucleon self-energy within the ladder approximation at zero temperature. They emphasized the need to correctly treat the pairing correlations contained in this approximation if hole-hole propagation is included in the kernel of the vertex function (thermodynamic T matrix). Benhar *et al.* [6] calculated spectral functions for nuclear matter using the hypernetted chain method. The spectral function and the nucleon momentum distribution in nuclear matter were calculated by Benhar *et al.* [7] at densities below the saturation density within orthogonal correlated basis functions theory. As a result, they find that with decreasing density the discontinuity at the Fermi surface decreases. This means that the momentum distribution does not approach the noninteracting response with decreasing density. This was interpreted as being due to the attraction in the NN interaction leading to the formation of ''bound pairs'' of nucleons. Van Neck *et al.* [8] use correlated basis functions theory with the Urbana v_{14} interaction to calculate the nuclear matter spectral function and momentum distribution below n_0. In agreement with the previous authors they found that the momentum distribution does not reach the noninteracting one with decreasing density. De Jong *et al.* [9] calculated the nucleon spectral function based on an extension of the relativistic Dirac-Brueckner scheme.

Finite temperature calculations of the nucleon self-energy

were carried out by Grangé *et al.* [10], Röpke *et al.* [11] (in connection with the EOS) and Köhler [12]. The latter author found a pronounced temperature dependence of the spectral function at the saturation density. Using the extended quasiparticle approximation for the nucleon spectral function Schmidt *et al.* [13] included the formation of two-nucleon correlations (in particular bound states) in the equation of state of nuclear matter. The finite temperature nucleon spectral function in the low-density region of nuclear matter was calculated by Alm *et al.* [14] demonstrating the necessity to include the contribution of two-nucleon bound states to the one-nucleon spectral function at low density. These authors find that genuine bound state formation in nuclear matter is only possible at extremely low densities ($n \leqslant 0.05 n_0$, $T = 10$ MeV). With increasing density the bound states are dissolved in the medium (Mott effect). However, the formation of two-nucleon pairs in the continuum as well as their possible Bose condensation [15] can take place at these higher densities as well. The necessity to include the deuteron singularity in the two-particle T matrix into the description of nucleon-nucleus scattering at low energies within the folding model was demonstrated by Arellano *et al.* [16].

Within this paper we would like to discuss the nucleon self-energy, spectral function, and momentum distribution at the saturation density and at finite temperatures. In particular, we will concentrate on low temperatures near the critical temperature for the superfluid phase transition in symmetric nuclear matter, which has a maximum of $\sim 5-6$ MeV at densities below n_0 [15]. This phase transition has recently been discussed by some authors in particular with respect to the possible formation of a condensate of neutron-proton-pairs in the ${}^3S_1 - {}^3D_1$ channel [17] and the relation to the Bose condensation of deuterons in low-density nuclear matter [18]. Moreover, Baldo *et al.* [19] suggest that this could be a possible mechanism of deuteron formation in heavy-ion reactions at intermediate energy. The onset of the superfluid phase is contained in the thermodynamic T matrix in the ladder approximation [15]. It manifests itself as a pole defining the critical temperature for the thermodynamic T matrix [20]. It could be shown that already above the critical temperature the T matrix shows a resonancelike behavior which could be understood as a precursor effect of the superfluid phase transition [21]. Consequently, near the critical temperature the self-energy and correspondingly the spectral function should reflect this resonancelike behavior of the T matrix. In this paper we will demonstrate how the T matrix, the nucleon self-energy and spectral function are changed when approaching the critical temperature for the superfluid phase transition from above.

In Sec. II we derive a set of self-consistent expressions for the retarded nucleon self-energy and the nucleon spectral function at finite temperature within the framework of Matsubara Green functions. In Sec. III the differences to the usual Brueckner theory generalized to finite temperatures are pointed out. Section IV contains results for the T matrix and the K matrix and the corresponding self-energies including the optical potential at finite T. Within Sec. V the corresponding spectral functions and occupation numbers are presented.

II. GREEN-FUNCTION FORMALISM AND APPROXIMATIONS

For the derivation of the self-energy and the spectral function we use the Matsubara Green-function technique as outlined in Ref. [22]. We put $\hbar, k_B = 1$ throughout the paper. From the definition of the one-particle spectral function $A(1,\omega) = i[G(1,\omega + i0) - G(1,\omega - i0)]$ and from the retarded self-energy Σ the spectral function according to the Dyson equation reads

$$A(1,\omega) = \frac{2\,\mathrm{Im}\Sigma(1,\omega)}{[\omega - p_1^2/2m - \mathrm{Re}\Sigma(1,\omega)]^2 + [\,\mathrm{Im}\Sigma(1,\omega)]^2}, \tag{1}$$

where $1 = \{p_1, \sigma_1, \tau_1\}$ denotes momentum, spin, and isospin of a single particle. The one-particle spectral function (1) fulfills the sum rule

$$\int \frac{d\omega}{2\pi} A(1,\omega) = 1. \tag{2}$$

It determines the macroscopic properties of the system such as the occupation n_1 of single-particle states given by

$$n_1(\mu,T) = \int \frac{d\omega}{2\pi} f(\omega) A(1,\omega), \tag{3}$$

where $f(\omega) = \{\exp[(\omega - \mu)/T] + 1\}^{-1}$ is the Fermi distribution. The equation of state of nuclear matter, where the nucleon density n is a function of the chemical potential μ and the temperature T, reads

$$n(\mu,T) = \frac{1}{\Omega} \sum_1 n_1(\mu,T), \tag{4}$$

with Ω being the normalization volume.

For the evaluation of the self-energy Σ in Eq. (1) approximations have to be made. We start from a cluster decomposition of the self-energy [23], which is given by the following set of diagrams:

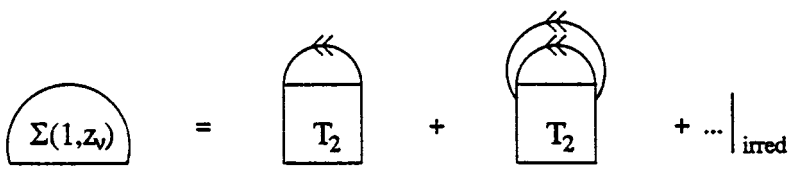

(5)

where z_ν is the fermionic Matsubara frequency. The cluster decomposition is appropriate for the consideration of n-particle correlations via the n-particle T matrix T_n. Within this paper we restrict to $n=2$, i.e., to two-particle correlations represented by the first diagram in Eq. (5). Within the ladder approximation the two-particle T matrix is given by

$$T(121'2',z)=V(121'2')+\frac{1}{\Omega}\sum_{3,4,5,6} V(1234) \times G_2(3456,z)T(561'2',z), \tag{6}$$

where the quantity G_2 is defined as the product of two full one-particle Green functions given in spectral representation as

$$G_2(121'2',z)=\int\frac{d\omega}{2\pi}\int\frac{d\omega'}{2\pi}\frac{1-f(\omega)-f(\omega')}{\omega+\omega'-z} \times A(1,\omega)A(2,\omega')\delta_{11'}\delta_{22'}. \tag{7}$$

Using the spectral representation for the one-particle Green function as well as for the T matrix [23] the first diagram in (5) yields

$$\Sigma(1,\omega+i0)=\frac{1}{\Omega}\sum_2\int\frac{d\omega'}{2\pi}A(2,\omega')\left(f(\omega')V_{\rm ex}(1212) -\int\frac{dE}{\pi}\frac{[f(\omega')+g(E)]{\rm Im}T_{\rm ex}(1212,E)}{E-\omega'-\omega-i0}\right), \tag{8}$$

where $f(\omega)$ is the Fermi distribution and $g(E)=\{\exp[(E-2\mu)/T]-1\}^{-1}$ the Bose distribution function for the two-nucleon states. $T_{\rm ex}$ and $V_{\rm ex}$ denote matrix elements of the retarded T matrix and of the potential including exchange.

The ladder T matrix equation (6,7) as well as the self-energy (8) contain the one-particle spectral function (1) and thus form a self-consistent set of equations. A solution of the complicated set of Eqs. (1), (6,7), and (8) can be achieved by iteration. In the first step of iteration we replace the spectral function in Eq. (8) by a quasiparticle spectral function

$$A^{\rm QP}(1,\omega)=2\pi\delta(\omega-\epsilon_1), \tag{9}$$

where the quasiparticle energy ϵ_1 is defined as

$$\epsilon_1=\frac{p_1^2}{2m}+{\rm Re}\Sigma(1,\omega)|_{\omega=\epsilon_1}. \tag{10}$$

Inserting the quasiparticle spectral function (9) in Eq. (7) results in the quasiparticle approximation for the two-particle T matrix (6). Within these approximations the following expressions for the imaginary and real part of the self-energy (8) are obtained:

$${\rm Im}\Sigma(1,\omega)=\frac{1}{\Omega}\sum_2[f(\epsilon_2)+g(\epsilon_2+\omega)]{\rm Im}T_{\rm ex}(1212,\epsilon_2+\omega) \tag{11}$$

and

$${\rm Re}\Sigma(1,\omega)=\frac{1}{\Omega}\sum_2\left(f(\epsilon_2){\rm Re}T_{\rm ex}(1212,\epsilon_2+\omega) -\mathbf{P}\int\frac{dE}{\pi}\frac{g(E){\rm Im}T_{\rm ex}(1212,E)}{E-\epsilon_2-\omega}\right), \tag{12}$$

where $\mathbf{P}$ denotes the Cauchy principal value. $T_{\rm ex}$ is calculated in the quasiparticle approximation. Rather than (12) we use in the numerical calculation the real part from the dispersion relation (Kramers-Kronig-relation) in the form

$${\rm Re}\Sigma(1,\omega)=\Sigma^{\rm HF}(1)+\mathbf{P}\int\frac{d\omega'}{\pi}\frac{{\rm Im}\Sigma(1,\omega')}{\omega-\omega'}, \tag{13}$$

where $\Sigma^{\rm HF}(1)$ denotes the Hartree-Fock shift. This was numerically checked to be equivalent with the explicit formula (12).

The bare nucleon-nucleon interaction was approximated by a separable ansatz

$$V_\alpha^{LL'}(p,p')=\sum_{i,j=1}^{\rm rank} w_{\alpha i}^L(p)\lambda_{\alpha ij}w_{\alpha j}^{L'}(p'). \tag{14}$$

The T matrix then can be given algebraically as

$$T_\alpha^{LL'}(p,p',P,E)=\sum_{ijk} w_{\alpha i}^L(p)[1-J_\alpha(P,E)]_{ij}^{-1} \times\lambda_{\alpha jk}w_{\alpha k}^{L'}(p'), \tag{15}$$

$$J_\alpha(P,E)_{ij}=\int\frac{d^3\mathbf{p}}{(2\pi)^3}\sum_{nL} w_{\alpha n}^L(p)\lambda_{\alpha in}w_{\alpha j}^L(p) \times\frac{\langle 1-f(\mathbf{P}/2+\mathbf{p})-f(\mathbf{P}/2-\mathbf{p})\rangle}{E-\epsilon(P/2+p)-\epsilon(P/2-p)}, \tag{16}$$

where $\langle\cdots\rangle$ denotes the usual angle averaging in the Pauli operator. Having the self-energy at our disposal the spectral function follows from Eq. (1). The quasiparticle energies ϵ_1 as defined by (10) were determined in Hartree-Fock approximation

$$\Sigma^{\rm HF}(1)=\frac{1}{\Omega}\sum_2 f(\epsilon_2)V_{\rm ex}(1,2,1,2). \tag{17}$$

With the T matrix (15) one is able to calculate the critical temperature for superfluidity using the Thouless criterion [20]. It has been demonstrated in Ref. [20] that this coincides with the critical temperature found in BCS theory. For the separable ansatz (14) it reads

$$\det[1-J_\alpha(P=0,E=2\mu,T=T_c)]_{ij}=0. \tag{18}$$

The Thouless criterion for nuclear matter has already been evaluated in Ref. [15].

III. SELF-ENERGY IN BRUECKNER THEORY

Brueckner theory is only applicable to zero-temperature systems. The near equivalence to Green-function results has been demonstrated in this case as already pointed out above. A $T>0$ extension of Brueckner theory was formulated by

Bloch and De Dominicis [24]. An obvious difference between the two approaches (Brueckner and Green function) is that the former only includes particle ladders, while the latter also includes hole ladders in defining the effective interaction. It is of some interest to numerically study the effect of this difference. We therefore define a Brueckner K matrix as in Eq. (6) with T replaced by K. The propagator (7) is however modified by the replacement

$$1-f(\omega)-f(\omega')\rightarrow[1-f(\omega)][1-f(\omega')]. \tag{19}$$

The self-energy (V_B) in Brueckner theory is given by [25]

$$V_B(1,\omega)=\frac{1}{\Omega}\sum_2\Bigg(f(\epsilon_2)K_{\rm ex}(1212,\epsilon_2+\omega) + \frac{1}{\Omega}\sum_{3,4}|K_{\rm ex}(1234,\epsilon_3+\epsilon_4)|^2 \times\frac{[1-f(\epsilon_2)]f(\epsilon_3)f(\epsilon_4)}{\omega+\epsilon_2-\epsilon_3-\epsilon_4-i\eta}\delta_{\mathbf{p}_1+\mathbf{p}_2,\mathbf{p}_3+\mathbf{p}_4}\Bigg). \tag{20}$$

For the discussion below, let us denote the two terms in Eq. (20) by V_B^1 and V_B^2. The second term, V_B^2, is often referred to as the Brueckner second-order rearrangement potential. At a temperature $T=0$ it is zero for states above the Fermi surface and negative for states below, while the first term is positive for states above and zero below the Fermi surface. As explained below, the retarded self-energy in (finite-temperature) Brueckner theory, denoted by Σ_B, is given by

$$\mathrm{Im}\Sigma_B(1,\omega)=\mathrm{Im}V_B^1(1,\omega)-\mathrm{Im}V_B^2(1,\omega), \tag{21}$$

$$\mathrm{Re}\Sigma_B(1,\omega)=\mathrm{Re}V_B(1,\omega)=\mathrm{Re}V_B^1(1,\omega) -\mathbf{P}\int\frac{d\omega'}{\pi}\frac{\mathrm{Im}V_B^2(1,\omega')}{\omega-\omega'}. \tag{22}$$

This quantity is to be compared to the Green function Σ defined in the previous section.

While Σ_B is calculated numerically according to Eqs. (20), (21), and (22), rewriting these expressions to parallel those in the last section would facilitate comparisons between the two formalisms. To this end, one can, invoking unitarity on the imaginary part of the second term of Eq. (20), write $\mathrm{Im}V_B$ as [25]

$$\mathrm{Im}V_B(1,\omega)=\frac{1}{\Omega}\sum_2[f(\epsilon_2)-\overline{g(}\epsilon_2,\omega)]\mathrm{Im}K_{\rm ex}(1212,\epsilon_2+\omega), \tag{23}$$

with

$$\overline{g(}\epsilon_2,\omega)=\frac{[1-f(\epsilon_2)]g(\epsilon_2+\omega)}{g(\epsilon_2+\omega)+1}=f(\epsilon_2)e^{-\beta(\omega-\mu)}. \tag{24}$$

Notice that at $2\mu=\epsilon_2+\omega$ where g has a singularity $\overline{g}$ is finite. It was argued in Ref. [27] that the Brueckner V_B should be identified with the chronological potential Σ^c which is related to Σ [26, 27] by

$$\mathrm{Im}\Sigma^c(1,\omega)=\tanh\left(\frac{1}{2}\beta(\omega-\mu)\right)\mathrm{Im}\Sigma(1,\omega). \tag{25}$$

In our notations here, this says, for $T>0$, one can obtain $\mathrm{Im}\Sigma_B$ from

$$\mathrm{Im}\Sigma_B=\frac{\mathrm{Im}V_B}{\tanh\left[\frac{1}{2}\beta(\omega-\mu)\right]}. \tag{26}$$

Now Eqs. (23) and (24) also give a simple relation between the two terms contributing to $\mathrm{Im}V_B(1,\omega)$:

$$\mathrm{Im}V_B^2(1,\omega)=-e^{-\beta(\omega-\mu)}\mathrm{Im}V_B^1(1,\omega). \tag{27}$$

It is then obvious that the division by the tanh function, in obtaining $\mathrm{Im}\Sigma_B$ from $\mathrm{Im}V_B$, is equivalent to just switching the sign of $\mathrm{Im}V_B^2(1,\omega)$:

$$\mathrm{Im}\Sigma_B(1,\omega)=(1+e^{-\beta(\omega-\mu)})\mathrm{Im}V_B^1(1,\omega), \tag{28}$$

as stated in Eq. (21) above.

An equivalent way of expressing the foregoing correspondence between $\mathrm{Im}V_B(1,\omega)$ and Green-function quantities is identifying $2i\mathrm{Im}V_B^1$ and $2i\mathrm{Im}V_B^2$ with, respectively, $\Sigma^<$ and $\Sigma^>$, the nonequilibrium extensions of which govern the loss and gain collision terms in a transport equation [28]. The on-shell version of this correspondence was pointed out by Cugnon *et al.* [29].

IV. RESULTS FOR THE *T* MATRIX (*K* MATRIX) AND THE NUCLEON SELF-ENERGY

In this exploratory calculation we used a rank one separable approximation (Yamaguchi potential [30]) as well as a rank two parametrization of Mongan [31]. The form factors of the barely attractive Yamaguchi potential are of the following form:

$$w_\alpha(p)=\frac{\lambda_\alpha}{p^2+\gamma^2}, \tag{29}$$

where the coupling constant and the effective range are given by

$$\lambda_\alpha=\begin{cases}12.3178(\mathrm{MeV\ fm^{-1}})^{1/2} & \alpha={}^1S_0\\ 14.6988(\mathrm{MeV\ fm^{-1}})^{1/2} & \alpha={}^3S_1\end{cases},$$

$$\gamma=1.4488\ \mathrm{fm^{-1}}. \tag{30}$$

The form factors for the rank two Mongan potential, which contains in addition to a long-range attractive a short-range repulsive term, have the same form as given in Eq. (29). The corresponding parametrization is given in Ref. [31]. For numerical convenience we restricted only to S waves ($^1S_0$, $^3S_1$) which give the dominant contribution to the T matrix at low energies.

As we are concerned within this paper with the modification of the self-energy near the critical temperature for the superfluid phase transition in symmetric nuclear matter, we first study the onset of superfluidity in the temperature-density plane of nuclear matter. In Fig. 1 the critical tem-

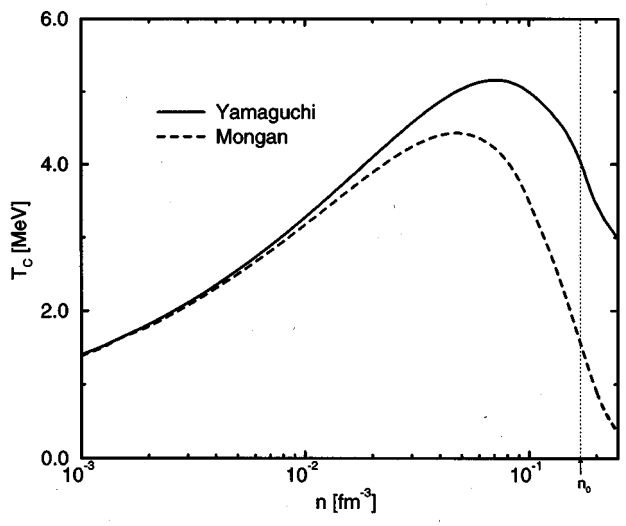

FIG. 1. The critical temperature for superfluidity in symmetric nuclear matter ($^3S_1$ channel) according to Eq. (18) as a function of density for the Yamaguchi and the Mongan potential. The saturation density n_0 is indicated.

perature for superfluidity (18) ($\alpha = {}^3S_1$) is given as a function of the density. The solid curve refers to the Yamaguchi potential whereas the dashed curve is for the Mongan interaction. Due to the repulsive component present in the Mongan interaction the critical temperature is reduced compared to the barely attractive Yamaguchi potential. These curves are in qualitative agreement with the calculations done in Ref. [15]. In the following calculations we fix the density to $n = n_0$ (dotted line in Fig. 1) and vary the temperature.

The key quantity for the calculation of the self-energy within the ladder approximation is the thermodynamic T matrix. In Fig. 2 the imaginary and the real part of the diagonal-matrix elements of the thermodynamic T matrix (triplet channel) of the Green-function theory (15) are given as a function of the energy argument at fixed relative momentum

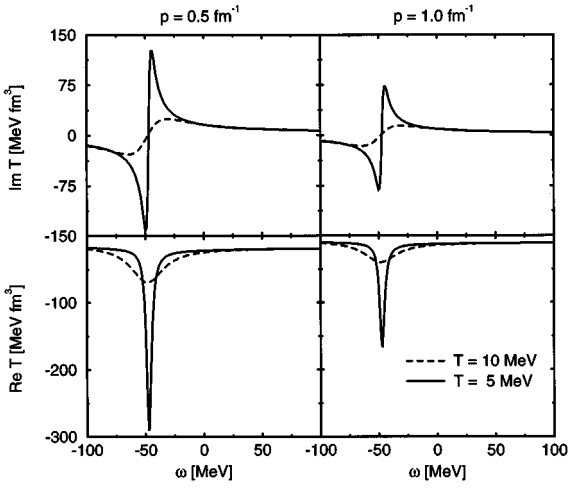

FIG. 2. Real and imaginary part of the diagonal elements of the thermodynamic T matrix (15) in the $^3S_1$ channel as a function of energy for temperatures far above and close to the critical temperature $T_c = 4.02$ MeV and for zero total momentum at the saturation density. The relative momenta were set to $p = 0.5$ and 1.0 fm^{-1}.

p and total momentum $P = 0$ as well as at a fixed chemical potential μ. The imaginary part shows a zero, which is located at $\omega = 2\mu$ independent on the temperature. This is due to the fact that the imaginary part of the T matrix (15,16) is proportional to

$$1 - 2f(\epsilon(p)) = g^{-1}(2\epsilon(p))f(\epsilon(p))f(\epsilon(p)), \qquad (31)$$

which is obviously zero at $2\epsilon(p) = 2\mu$ for any temperature. With decreasing temperature the slope of the imaginary part of the T matrix at $\omega = 2\mu$ increases; at temperatures near T_c ($T_c = 4.02$ MeV in our case) it has a characteristic principal value structure. The real part develops the corresponding peak at $\omega = 2\mu$, while approaching the critical temperature from above. Finally at $T = T_c$ the real part of the T matrix diverges in accordance with the Thouless criterion [20].

The results of Fig. 2 can be compared with the $T = 0$ results by Ramos *et al.* [32]. They also find a pairing instability at $T = 0$ and $\omega = 2\epsilon_F$ which is most pronounced for small total momenta. The difference compared to our results lies in the fact that although their imaginary part goes to zero at $\omega = 2\epsilon_F$ as well, it does not change sign at this energy as it does in our calculations. This is due to the fact that in Ref. [32] the Galitski form of the two-particle propagator in the kernel of the T matrix is used [22] whereas we use the Kadanoff-Baym form [33], which results in the retarded T matrix instead of the chronological one used in Ref. [32]. In the limit $T \to 0$ both differ only in the sign of the imaginary part for $\omega > 2\epsilon_F$. Consequently both definitions differ also in the sign of the corresponding self-energies at $T = 0$. At finite T the retarded self-energy discussed so far and the chronological self-energy as derived from the Feynman-Galitski T matrix [26] are related by Eq. (25). However, with this difference in mind we can conclude that the pairing instability at $T = T_c$ is in qualitative agreement with the corresponding instability at $T = 0$ observed in Ref. [32]. However, a proper treatment of the pairing correlations below T_c demands the inclusion of a finite gap in the single-particle propagators. This has to be determined consistently from a combination of the BCS theory with the T-matrix approximation. Such a treatment known as quasiparticle-random-phase approximation [34] has recently been applied to the one-dimensional Fermi gas [35].

To compare with the Brueckner theory the respective key quantity is the K matrix. In Fig. 3 the K-matrix elements of the Brueckner theory are given for the same set of parameters. The imaginary part of the K matrix does not change sign in contrast to the T-matrix elements (Fig. 2). This is due to the fact that in this case the Pauli blocking (19) is positive in contrast to the Pauli-blocking term (31), which changes sign at $2\epsilon(p) = 2\mu$. For low temperatures the imaginary part is effectively zero for energies below this particular energy. For energies above this value a pronounced maximum develops. This gives the corresponding maximum in the real part of the K matrix. However, no critical temperature can be found where the K matrix diverges as found for the T matrix (Thouless criterion). Thus, the different Pauli operator (19) in the K matrix leads to considerable deviations from the T-matrix case in particular in the limit of low temperatures.

In order to calculate the spectral function it is necessary to evaluate the off-shell self-energy, which itself has some in-

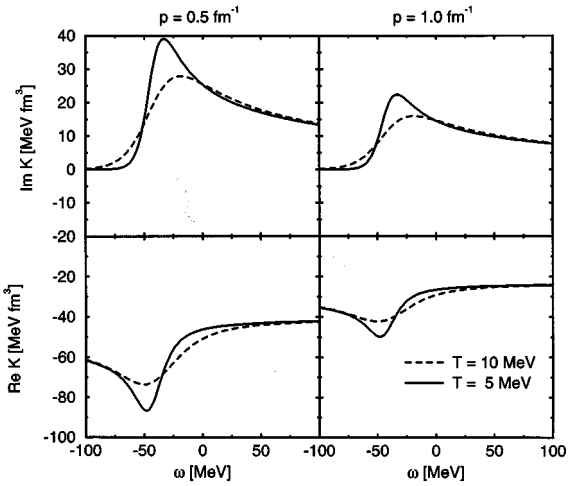

FIG. 3. Real and imaginary part of the diagonal elements of the thermodynamic K matrix ($^3S_1$) from Brueckner theory plotted for the same parameters as in Fig. 2.

teresting features. In Fig. 4 the imaginary part of the retarded self-energy (11) is given as a function of ω at $p_1=0$ and $n=n_0$. The results are plotted for various temperatures. At the highest temperature $T=20$ MeV (dotted curve) the self-energy is rather smooth. It gives a nonzero contribution for energies $\omega>-200$ MeV, develops a maximum near $\omega=-100$ MeV and then starts decreasing slowly. In the $T=10$ MeV case we find two additional extrema: a minimum at the the chemical potential $\omega=\mu\approx-23$ MeV and a second maximum at $\omega_0=2\mu-\epsilon(p_1)\approx35$ MeV. Decreasing the temperature further this behavior gets still more pronounced. At the minimum the value of the imaginary part is drastically reduced; however, it still has a finite value and will reach zero only in the limit $T\to0$ (see discussion of Fig. 5). The second maximum gets more pronounced as well. At a temperature $T=4.1$ MeV, close to the critical temperature $T_c=4.02$ MeV, one observes a pronounced peak.

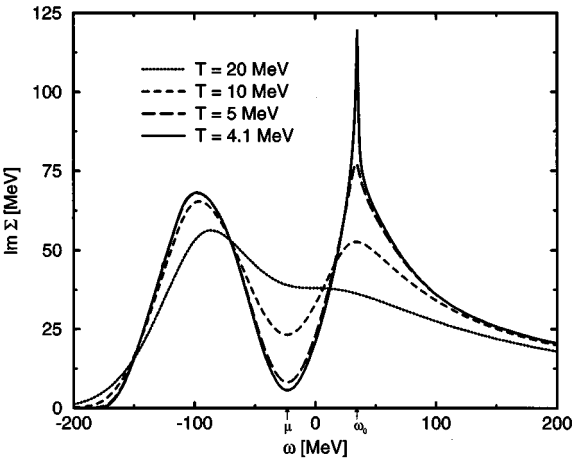

FIG. 4. Imaginary part of the nucleon self-energy (11) at the saturation density n_0 as a function of energy for momentum $p_1=0$. The self-energy is given for several temperatures above the critical temperature for superfluidity ($T_c=4.02$ MeV). The chemical potential $\mu=-23.5$ MeV ($T=4.1$ MeV) and the location of the pairing peak at $\omega_0=2\mu-\epsilon_1=35.6$ MeV are indicated.

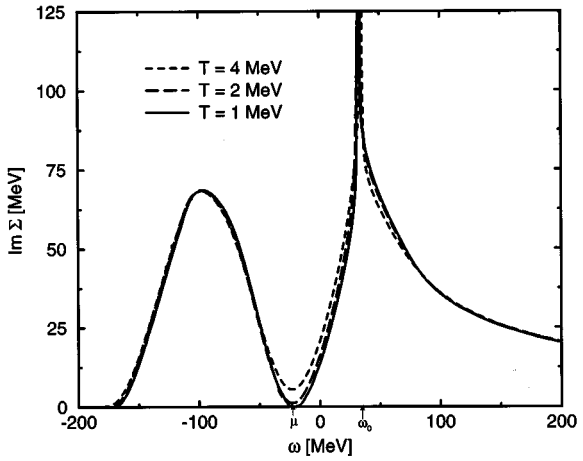

FIG. 5. The same quantity as in Fig. 4 for temperatures below the critical temperature $T_c=4.02$ MeV. Again the chemical potential $\mu=-22.2$ MeV ($T=1$ MeV) is indicated.

This particular behavior can be traced back to the behavior of the T matrix (15) at low temperatures. It has been demonstrated in Ref. [21] that ImT has a zero at the particular energy value $z=2\mu$ for pairs with zero total momentum (compare also Fig. 2). This compensates for the Bose singularity in the imaginary part of the self-energy (11) rendering Im Σ at this energy finite. However, in addition a critical temperature can be found such that the real part of the T matrix becomes singular at the same energy (Fig. 2). As has been shown in Ref. [21] this critical temperature coincides with the one for the superfluid phase transition in agreement with the BCS theory. In fact, the singularity in the T matrix is nothing but the well-known Thouless criterion [20] for superfluidity. If this critical temperature is reached the above-mentioned compensation does no longer hold (see also Ref. [21]) and the singularity in the T matrix leads to a corresponding singularity in the imaginary part of the self-energy. The singularity is located at an energy $\omega_0=2\mu-\epsilon_1$. This is readily to be seen if one restricts to the pole part of the T matrix with total momentum $P=0$. Then the integration over p_2 in (11) can be carried out directly yielding a δ peak in Im Σ at the energy ω_0. This shows that the singularity in the imaginary part of the self-energy, which occurs for $T\to T_c$ is a direct consequence of the pole in the T matrix at $T=T_c$, indicating the onset of superfluidity.

In Fig. 5 we continued the evaluation of the imaginary part of the self-energy for temperatures below T_c, disregarding for the moment the pairing instability. This allows us to demonstrate that for $T\to0$ indeed the value of the imaginary part of Σ at the minimum ($\omega=\mu=-23$ MeV) approaches zero, in accordance with zero-temperature calculations of various authors [5, 36]. This zero of the imaginary part of the self-energy at $\omega=\mu$ is a wellknown property at zero temperature leading to the fact that particles at the Fermi surface have infinite lifetime, i.e., they are good quasiparticles. According to the Hugenholtz-van-Hove theorem the chemical potential coincides with the binding energy per nucleon. The empirical value for this quantity at saturation is $E_B^0/A=-16$ MeV. The quadratic dependence of ImΣ around $\omega=\mu$ at $T=0$ demonstrated in Ref. [37] is also found in our

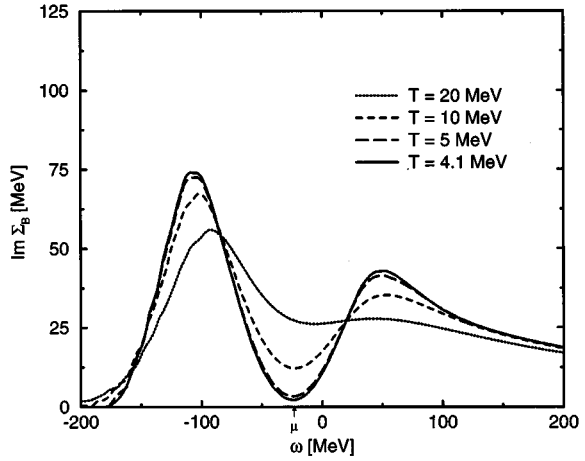

FIG. 6. The imaginary part of the nucleon self-energy at the saturation density calculated in Brueckner theory [Eqs. (21)] for the same parameters as in Fig. 4.

numerical calculations. With increasing temperature a nonzero value for $\mathrm{Im}\Sigma$ is obtained at $\omega=\mu$, however up to temperatures $T\leqslant 20$ MeV (see Fig. 4) a pronounced minimum is reminiscent of the zero-temperature property. At all temperatures $T<T_c$ the pairing instability shows up at $\omega_0=2\mu-\epsilon_1=35$ MeV. This pairing instability indicates the breakdown of the T-matrix approximation in the vicinity of ω_0 at temperatures below T_c. A consistent treatment requires the inclusion of the BCS gap for temperatures below T_c. Such a complicated calculation has not yet been carried out. The $T=1$ MeV curve in Fig. 5 is in qualitative agreement with the calculation of Ref. [4] except at energies around $\omega\approx 35$ MeV. There we find the additional peak due to the pairing singularity in the T matrix discussed above.

In Fig. 6 the imaginary part of the self-energy $\mathrm{Im}\Sigma_B$ (21) is given as a function of energy for the same parameters as in Fig. 4. For $T=20$ MeV $\mathrm{Im}\Sigma_B$ is in qualitative agreement with the corresponding curve in Fig. 4. With decreasing temperature the qualitative behavior is similar to the Green function case given in Fig. 4 except in the energy range around ω_0. Whereas a strong singularity is seen in Fig. 4 for temperatures close to T_c only a small maximum is found in the Brueckner case for the same temperature. As discussed above this singularity is due to the pairing singularity in the T matrix and occurs at the critical temperature defined by the Thouless criterion. This behavior does not show up in the Brueckner theory.

Figure 7 gives a direct comparison between the imaginary parts of the self-energy, calculated in the T matrix and the Brueckner approximations, respectively. The upper curves show the case at $T=20$ MeV. While for energies below $\omega=-100$ MeV and above $\omega=100$ MeV the two curves almost coincide, the imaginary part of the Brueckner self-energy lies below the one from the T-matrix calculation in the energy range between -100 and 100 MeV. An analogous result has been found in the zero-temperature case by Köhler [4]. In the $T=4.1$ MeV case (slightly above T_c) we observe a similar relation between the two approximations. However, at energies around ω_0 the Green-function self-energy shows the pairing singularity, which is absent in the Brueckner calculation.

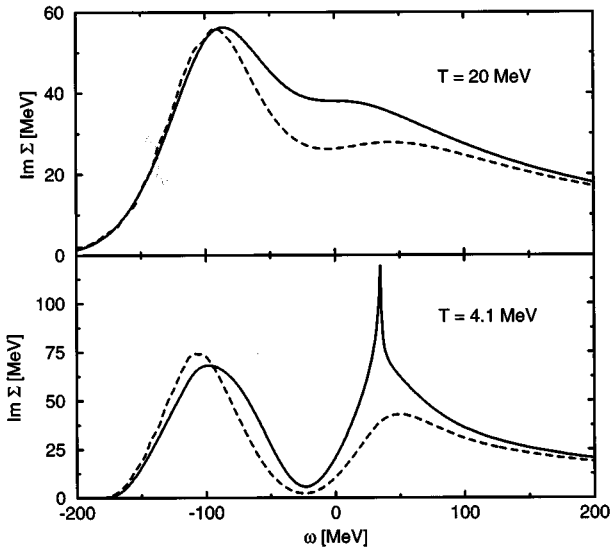

FIG. 7. Direct comparison of the imaginary part of the self-energy in Brueckner theory (dashed curves) and Green-function theory (solid curves) for temperatures $T=20$ and $T=4.1$ MeV.

In Fig. 8 the same quantity as in Fig. 4 is given using the Mongan potential instead of the Yamaguchi potential used throughout the rest of the paper. The purpose is to demonstrate the influence of the repulsive part of the nucleon-nucleon interaction on the self-energy. The repulsion leads to a lower critical temperature ($T_c=1.58$ MeV) as compared to the barely attractive case ($T_c=4.02$ MeV). The temperature dependence of $\mathrm{Im}\Sigma$ does not change qualitatively compared to Fig. 4. Thus, we suppose that the behavior discussed above also holds for more realistic interactions, such as the Paris potential [38] as used, e.g., in Ref. [21].

In addition to the imaginary part the real part of the self-energy contains important information, its on-shell part de-

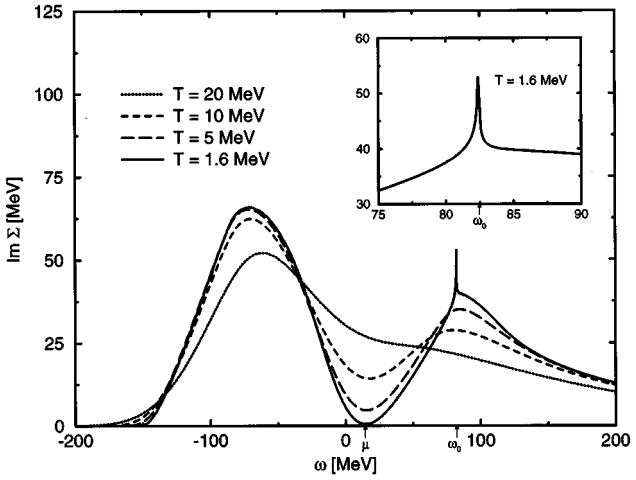

FIG. 8. The imaginary part of the nucleon self-energy at the saturation density for the Mongan NN interaction. The critical temperature in this case has a smaller value ($T_c=1.58$ MeV) than for the Yamaguchi potential. Like in Fig. 4 the self-energy is given for several temperatures above and close to the critical temperature for superfluidity. The chemical potential $\mu=14.68$ MeV and the energy $\omega_0=82.46$ MeV is indicated. The inset shows the region around ω_0 in detail.

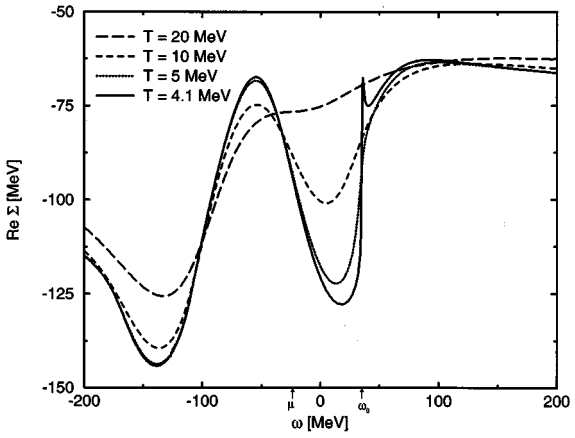

FIG. 9. The real part of the off-shell nucleon self-energy calculated from the imaginary part according to Eq. (13) as a function of energy for $n=n_0$ and the same temperatures as in Fig. 4.

fines the optical potential for the nucleon in nuclear matter. In Fig. 9 the energy dependence of the real part of the self-energy as calculated from Eq. (13) is shown for the same parameters as used in Fig. 4. Again there is a relatively smooth behavior for the $T=20$ MeV case. With decreasing temperature a second minimum is found for energies below ω_0. Please note that for $T=4.1$ MeV (close to $T_c=4.02$ MeV) a principle-value-like behavior around $\omega=\omega_0$ is found. This a direct consequence of the corresponding pairing peak in the imaginary part of the self-energy at $\omega=\omega_0$ (see Fig. 4).

In Fig. 10 the real part of the on-shell self energy, i.e., the real part of the optical potential, is given as a function of the momentum p. The upper curve shows a calculation using only the first term in Eq. (12). This is a standard approximation often used to calculate the optical potential in nuclear matter [13,39,40]. With decreasing temperature one observes a pronounced minimum near the Fermi energy, which has been observed in Ref. [13] and related to the inclusion of hole-hole scattering in the Pauli operator. However, using the full expression of Eq. (12) for the evaluation of the optical potential the behavior at low temperatures is changed. A particular structure is found around momenta $p=p_F$ which is enhanced with decreasing temperature. If one studies the behavior of the real part in detail, one finds, that the $^3S_1$ channel of the T matrix is responsible for this anomalous behavior. We suppose, that the pairing peak in the imaginary part $\mathrm{Im}\Sigma(p,\omega)$ at temperatures $T\rightarrow T_c$, present also at finite momenta p, leads to a corresponding principal-value-like structure in the real part of the optical potential. Restricting to the pole part of the T matrix this behavior can be shown using the dispersion relation between the real and imaginary parts of the self-energy. Consequently for the on-shell self-energy $\mathrm{Re}\Sigma$ this leads to the wiggle at $p=p_F$.

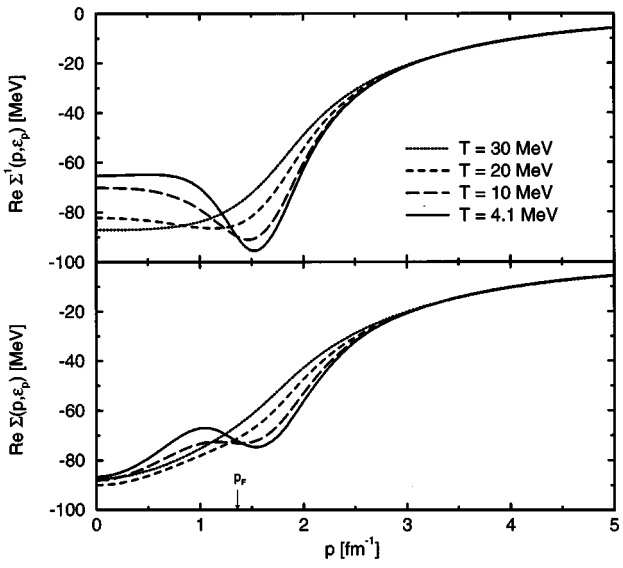

FIG. 10. The real part of the on-shell nucleon self-energy as a function of the momentum p for $n=n_0$ and different temperatures according to Eq. (12). The upper figure was a calculation using only the first term of Eq. (12) denoted as $\mathrm{Re}\Sigma^1$. The lower plot shows the result of the full expression. The Fermi momentum is indicated as p_F.

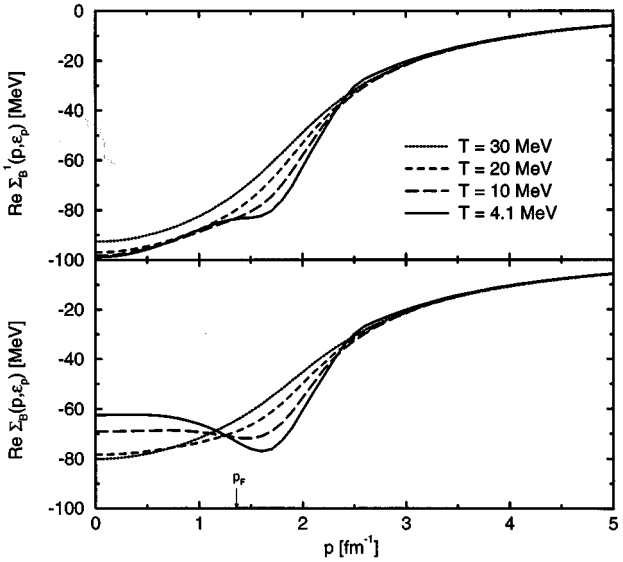

FIG. 11. The real part of the on-shell nucleon self-energy calculated with the Brueckner K matrix. The parameters are the same as in Fig. 10. While the upper figure shows the results only with the first term of Eq. (22) denoted as $\mathrm{Re}\Sigma_B^1$ the lower part shows the results of the full calculation.

Figure 11 shows the same quantity calculated from the Brueckner theory. The upper plot denoted as $\mathrm{Re}\Sigma_B^1$ shows the temparature behavior of the first-order Brueckner term [Eq. (22)]. For the lowest temperature ($T=4.1$ MeV) one observes a plateaulike behavior around the Fermi momentum. Using the full expressions (lower plot) the repulsive second-order contribution leads to a different behavior at low temperatures, which is characterized by a strong enhancement for low momenta and a corresponding minimum for momenta $p>p_F$.

A particular behavior of the optical potential for momenta around $p=p_F$ has also been found in Refs. [39, 41]. In Ref. [41] a plateaulike behavior was related to the behavior of the effective mass at the Fermi surface. In [39] it was shown that a nonmonotonous behavior around p_F (anomaly) was entirely due to the strong attraction in the $^3S_1-{}^3D_1$ channel

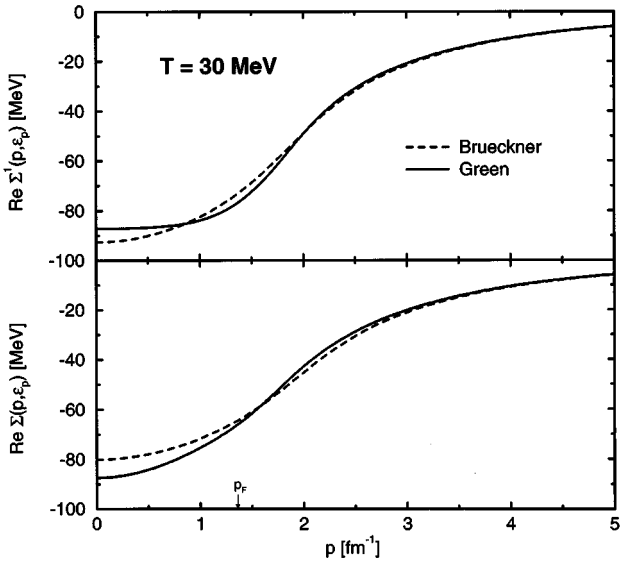

FIG. 12. The real part of the on-shell nucleon self-energy calculated in T matrix and Brueckner approximations, respectively, for temperature $T=30$ MeV.

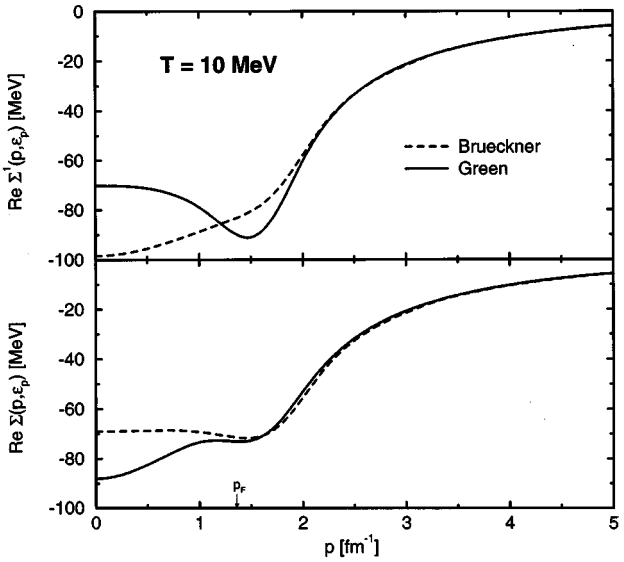

FIG. 13. The same figure as Fig. 12 for temperature $T=10$ MeV.

and that it was enhanced if the density was decreased below $n=n_0$. According to our understanding the anomaly observed in Ref. [39] is probably as well due to the pairing instability [42] discussed above.

In Figs. 12–14 we give a direct comparison between the Green-function theory and Brueckner theory with respect to the real part of the on-shell self-energy for different temperatures. The upper curves correspond to the first term in Eqs. (12) and (22), respectively. As the form of these expressions coincides, the differences between Green-function and Brueckner theory in this case are entirely due to the different Pauli operators in the T matrix and K matrix, respectively [compare Eq. (19)]. The lower curves show the result of the full expressions (12) and (22). In Fig. 12 we give the results for temperature $T=30$ MeV. The differences between the two approaches are not very pronounced for this temperature, except for low momenta. With respect to $\mathrm{Re}\Sigma^1$ the Green-function curve is slightly enhanced compared to the Brueckner curve for momenta $p\simeq p_F$ and slightly reduced below. This behavior is reversed for the lower curves. In Fig. 13 ($T=10$ MeV) the differences between the two theories are much more pronounced. The different form of the Pauli operator results in a nonmonotonous behavior for the Green-function curve showing a pronounced minimum around $p=p_F$. In contrast the Brueckner curve is monotonously decreasing. A behavior like this has been observed in Ref. [13]. For the full expressions the differences between both theories are less pronounced showing an enhancement of the Green-function curve with respect to the Brueckner curve for momenta $p<p_F$. In Fig. 14 the temperature ($T=4.1$ MeV) is close to the critical temperature $T_c=4.02$ MeV. One observes basically the same behavior as in Fig. 13, although the differences are still more enhanced.

In Fig. 15 the imaginary part of the on-shell self-energy (optical potential) is given as a function of momentum for various temperatures. The upper graph shows the contribution of the first term in Eq. (11) only. One observes a pronounced temperature dependence for momenta below $p=2$ fm^{-1} leading to a decrease with temperature towards a minimum near $p=p_F$. The lower graph displays the full contribution for the imaginary part (11). Again, one notes a strong temperature dependence below $p=2$ fm^{-1}. For momenta around the Fermi momentum a pronounced minimum is exhibited with decreasing temperature. The value of $\mathrm{Im}\Sigma$ at $p=p_F$ tends to zero for $T\rightarrow 0$. In Fig. 16 the imaginary part of the on-shell self-energy calculated in Brueckner theory $\mathrm{Im}\Sigma_B$ is given as a function of momentum for the same parameters as in Fig. 15. The upper plot displays the first term of Eq. (21). Again, we observe a strong decrease with temperature for momenta below $p=2$ fm^{-1} as in Fig. 15. However, due to the use of the different Pauli operator in the K matrix $\mathrm{Im}\Sigma_B^1$ is basically zero for momenta $p<p_F$ in the limit of low temperatures. No minimum can be observed. In the lower graph the full contribution of $\mathrm{Im}\Sigma_B$ (21) is shown.

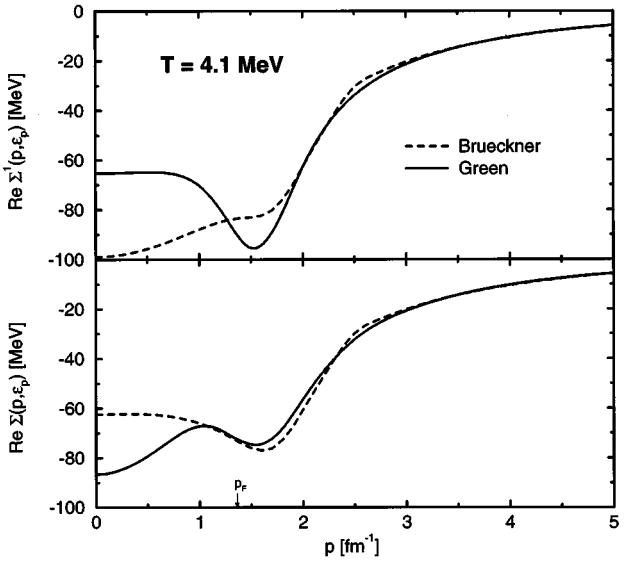

FIG. 14. The same figure as Fig. 12 for temperature $T=4.1$ MeV.

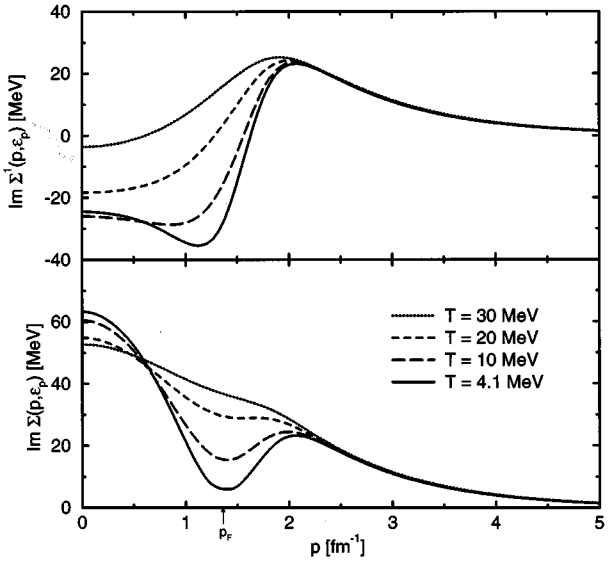

FIG. 15. The imaginary part of the on-shell self-energy as a function of p at n_0 for the same temperatures as in Fig. 10, according to Eq. (11). The upper figure was a calculation using only the first term of Eq. (11) denoted as $\mathrm{Im}\Sigma^1$. The lower plot shows the result of the full expression. The Fermi momentum is indicated as p_F.

One notes, that the temperature dependence for momenta around p_F is in qualitative agreement with the Green-function result (lower curve of Fig. 15). However, for momenta $p \leqslant 1$ fm^{-1} the temperature behavior is reversed compared to the Green-function case. Please note, that it is in the same momentum range, where one notes pronounced deviations in the real part of the optical potential at low temperatures (compare lower part of Fig. 14). The Brueckner results can be compared with the calculation of $\mathrm{Im}V_B(1,\epsilon_1)$ in Ref.

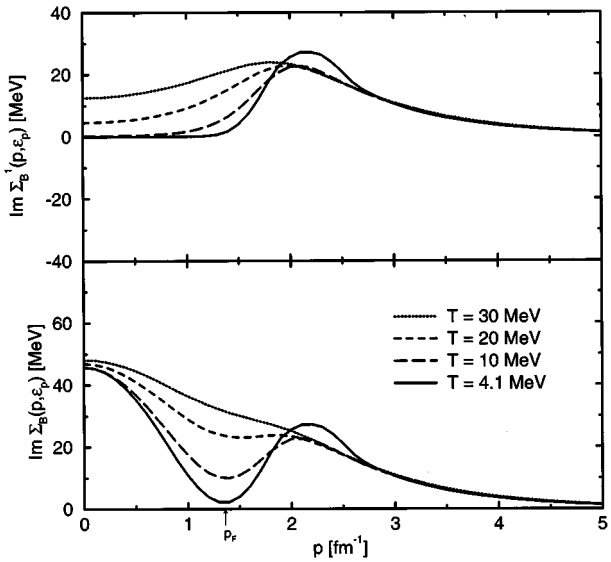

FIG. 16. The imaginary part of the on-shell nucleon self-energy calculated with the Brueckner K matrix. The parameters are the same as in Fig. 15. The upper figure shows the results only with the first term of Eq. (21) denoted as $\mathrm{Im}\Sigma_B^1$. The lower part shows the results of the full calculation (21).

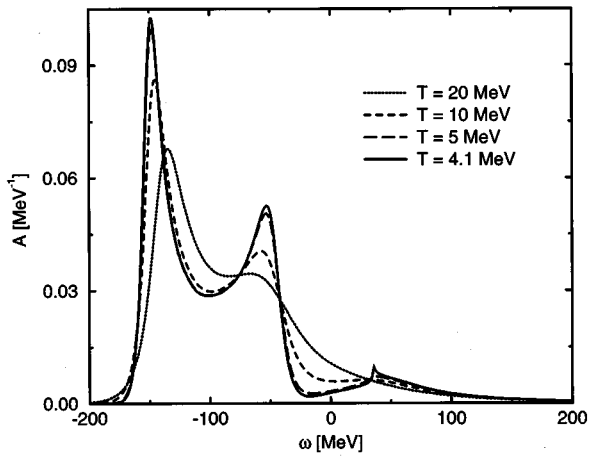

FIG. 17. The nucleon spectral function at the saturation density as a function of energy for momentum $p_1 = 0$. The temperatures are the same as in Fig. 4.

[10]. Taking into account the relation between $\mathrm{Im}\Sigma_B$ and $\mathrm{Im}V_B$ (see Sec. III) one notes the qualitative agreement of the two calculations.

Summarizing, one observes pronounced differences between the optical potential at low temperatures calculated in Green-function theory and Brueckner theory, respectively. These show up at momenta below the Fermi momentum. For the full expressions (lower curves) these differences are due to higher-order terms in the Green-function approximation, not included in the second-order Brueckner calculation (see also Ref. [25]).

V. SPECTRAL FUNCTION AND MOMENTUM DISTRIBUTIONS

From the off-shell self-energy the nucleon spectral function is calculated using Eq. (1). In Fig. 17 the nucleon spectral function is plotted as a function of energy ω for zero momentum $p_1 = 0$ at a density $n = n_0$ and for the same temperatures as given in Fig. 4. For $T = 20$ MeV one observes a quasiparticle peak at energies $\omega = -150$ MeV and a background contribution extending up to energies $\omega \approx 200$ MeV. With decreasing temperature the quasiparticle peak is slightly shifted towards higher energies and its width is reduced. This reduction is due to the fact that with decreasing temperature the imaginary part reaches zero at higher energies (compare Fig. 4). In addition a second maximum forms at lower energies. This can be compared with the zero-temperature results in Ref. [4] for the spectral function at $p = 0$. Using Green-function theory they also arrive at a spectral function with two peaks of comparable size which are located at approximately the same energies as given in Fig. 17 in the $T = 4.1$ MeV case.

The temperature dependence of the spectral function is not as drastic as one could expect from the change in the self-energy with temperature (Fig. 4). Near the critical temperature the tail of the spectral function at higher energies shows additional smaller maxima, which result from the pronounced structures in the real part of the self-energy. These in turn are due to the singular behavior of the imaginary part at $\omega = 2\mu - \epsilon_1$.

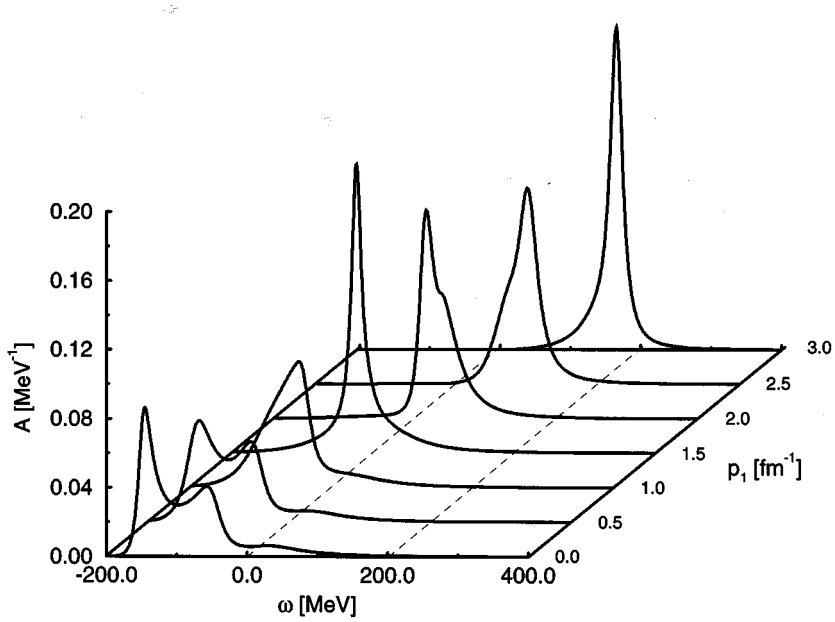

FIG. 18. The nucleon spectral function at saturation density and $T=10$ MeV in the energy-momentum plane.

In Fig. 18 the energy and momentum dependence of the spectral function is given at $n=n_0$ and $T=10$ MeV. One observes that the double-peak structure found at $p=0$ vanishes with increasing momentum. A single maximum remains for $p_1>0.7$ fm^{-1} which can be identified with the quasiparticle peak. The width of this peak is reduced at $p=p_F$ due to the minimum in ImΣ at the chemical potential. For larger momenta the peaks are broadened again until for very high momenta the width is reduced again. The latter behavior is due to the fact that for very high momenta the influence of the medium represented by the self-energy becomes negligible. Please note, that for our choice of the nucleon-nucleon interaction there is no high-momentum tail of the spectral function because it is barely attractive.

In order to demonstrate the influence of correlations on the nucleon occupation numbers, the spectral function can be used to determine this quantity. In Fig. 19 the temperature dependence of the nucleon momentum distribution (occupation numbers) $n(p)$ (3) is given at a fixed density $n=n_0$. The correlated occupation number (full line) is compared to the corresponding Fermi distribution function (dashed line). In the $T=5$ MeV case we observe a strong depletion for momenta below the Fermi momentum with a value of $n(p=0)=0.78$ compared to 1 for the noninteracting case. Above the Fermi surface we find a corresponding enhancement of the interacting occupation numbers compared to the noninteracting up to about $p=2$ fm^{-1}. For $T=10$ MeV the depletion is less pronounced $[n(0)=0.82]$. This tendency towards the noninteracting occupation numbers is continued is the case of $T=30$ MeV. With further increasing temperature the interacting response approaches the noninteracting one. Using the Brueckner K matrix in Ref. [43] the finite temperature occupation numbers are evaluated which are in reasonable agreement with our results as well with the calculations of Ref. [10].

In Fig. 20 the density dependence of $n(p)$ at fixed T (10 MeV) is shown. For the sake of a better comparability the curves are normalized to p/p_F. When going to densities above n_0 $(n/n_0=1.32)$ one observes a lower depletion $[n(p=0)=0.85]$ compared to $n(p=0)=0.82$ at $n=n_0$. The same tendency has also been observed in Ref. [43], although at a higher temperature (30 MeV). Going to lower densities $(n/n_0=0.61)$ we find the astonishing result that the depletion at low p is further enhanced $[n(p=0)=0.78]$. On the other hand this corresponds to the zero-temperature results of Refs. [7,8] indicating that the momentum distribution does not approach the noninteracting one in the limit of zero density. In Ref. [8] the depletion at $T=0$ and $p=0$ stays rather constant for densities between n_0 and $n_0/2$ at a value of $n(p=0)=0.86$. The authors of Ref. [8] interpret this result as being due to the attractive part of the nucleon-nucleon interaction leading to the formation of bound pairs at low densities.

VI. SUMMARY AND CONCLUSIONS

Using the Matsubara Green-function approach, self-consistent expressions for the nucleon self-energy and the nucleon spectral function for nuclear matter at finite temperature were derived. The self-energy and the nucleon spectral function at the saturation density were calculated in first iteration starting from the quasiparticle spectral function. The variation of these quantities with temperature was studied for temperatures close to the critical temperature T_c for the superfluid phase transition in symmetric nuclear matter. We found that approaching the critical temperature from above a singularity develops in the imaginary part of the self-energy. It was shown that this singularity is a direct consequence of a corresponding pole in the T matrix at the energy $E=2\mu$, which indicates the onset of a superfluid phase at $T=T_c$ [20]. Thus, the modification of the self-energy near T_c can be understood as a precursor effect of the superfluid phase transition in nuclear matter. Another effect which was discussed as being related to the pairing instability in the $^3S_1$-$^3D_1$ channel is the occurrence of a wiggle around $p=p_F$ in the real part of the on-shell self-energy, especially pronounced when approaching T_c from above. A similar effect although less pronounced was also found in the Brueckner calculation.

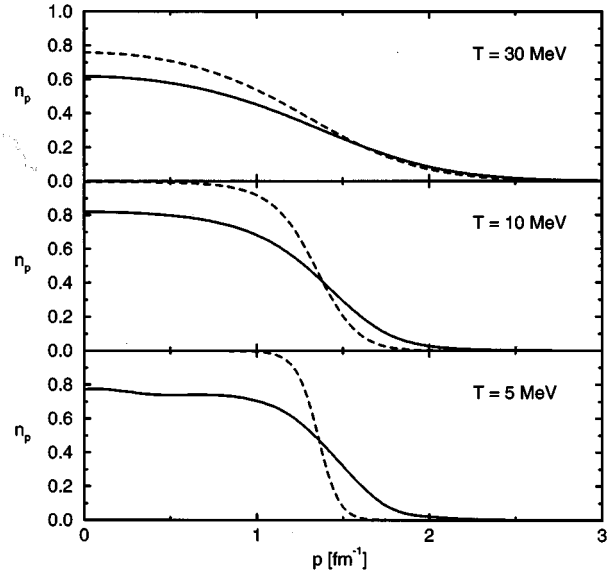

FIG. 19. Occupation numbers at saturation density for different temperatures. The dashed curves represent the uncorrelated occupation numbers, i.e., the corresponding Fermi distribution.

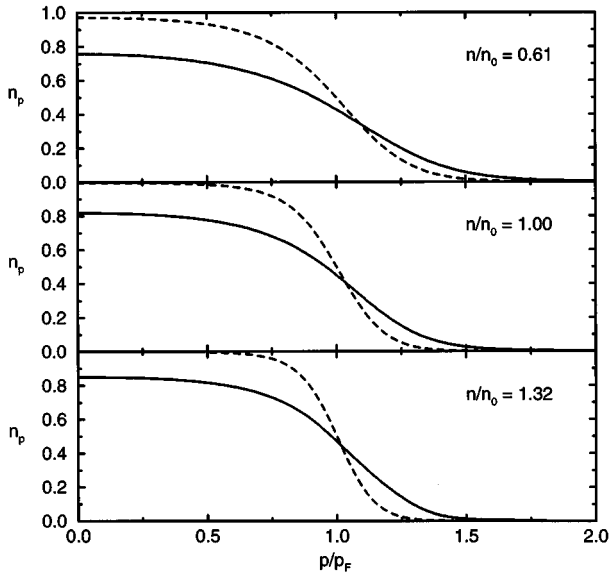

FIG. 20. Occupation numbers at $T=10$ MeV for density values around the saturation density. Again the dashed curves represent the noninteracting case.

The temperature dependence of the spectral function has been investigated for temperatures above the critical temperature. Despite the strong modification of the self-energy there is no such drastic modification of the spectral function when approaching T_c from above. This is consistent with the fact that below T_c the condensate part of the T matrix is proportional to the square of the gap and consequently vanishes at the critical temperature.

The momentum dependence of the spectral function shows considerable deviations from the quasiparticle behavior at small momenta, whereas the quasiparticle picture holds approximately for momenta around $p=p_F$ as well as for large p.

The occupation numbers were calculated from the spectral function at some finite temperature and density. It could be shown that with increasing temperature the noninteracting occupation number is approached. The depletion of the occupation numbers is enhanced with decreasing density at finite temperature.

We would like to mention some open questions related to our calculation of the nucleon spectral function: The first question is related to the model interaction we used in our exploratory calculation of the self-energy and spectral function. For the energy and momentum range investigated in this paper the important features of the self-energy obtained using the simple model interaction of Yamaguchi type were also found using a rank two Mongan interaction. It is supposed that these features remain of relevance also for more realistic potentials [38].

The second question is related to the problem of self-consistency. In principle, the spectral functions have to be iterated until self-consistency is reached. It remains to be seen, to what extent the features of the first iteration obtained in this calculation will also be found in a fully self-consistent calculation.

The third question concerns a consistent description of the system below T_c, where the consistent inclusion of a finite gap is necessary for the evaluation of the spectral function. In principle, our calculation is restricted to temperatures above the critical temperature for superfluidity. The Thouless criterion indicates the instability of the normal quasiparticle state with respect to the onset of superfluidity. A consistent treatment below T_c has to be based, e.g., on a BCS quasiparticle basis with a finite gap. Up to now such a calculation has not been carried out for nuclear matter. Instead, in most of the approaches at zero temperature the implications of the pairing singularity for the self-energy were neglected. However, in a series of papers Vonderfecht *et al.* [5] stressed the need to properly take into account the T-matrix singularity, discussed above, which is present at temperatures below T_c.

In conclusion we evaluated the nucleon self-energy and spectral function for finite temperature. We compared the calculations within the Green-function approach with a finite-temperature generalization of the Brueckner theory. Special emphasis was put on the behavior of these quantities near the critical temperature for the onset of superfluidity in nuclear matter. Within the Green-function approach the pairing singularity in the T matrix at the critical temperature generates a corresponding singularity in the imaginary part of the self-energy. The nonmonotonous behavior (anomaly) of the real part of the optical potential for momenta $p\sim p_F$ could also be related to the pairing singularity. The spectral function at finite temperature shows a complex energy dependence, which cannot be generated from an energy-independent width.

All the features discussed above cannot be incorperated into a simple quasiparticle description. Thus, the nucleon spectral function should be the appropriate quantity for the description of hot and dense nuclear matter.

[1] O. Benhar, A. Fabrocini, S. Fantoni, G.A. Miller, V.R. Pandharipande, and I. Sick, Phys. Rev. C **44**, 2328 (1991), and references therein.
[2] O. Benhar, A. Fabrocini, and S. Fantoni, Nucl. Phys. **A505**, 267 (1989).
[3] M. Baldo, I. Bombaci, G. Giansiracusa, U. Lombardo, C. Mahaux, and R. Sator, Nucl. Phys. **A545**, 741 (1992).
[4] H.S. Köhler, Phys. Rev. C **46**, 1687 (1992).
[5] B.E. Vonderfecht, W.H. Dickhoff, A. Polls, and A. Ramos, Nucl. Phys. **A555**, 1 (1993).
[6] O. Benhar, A. Fabrocini, and S. Fantoni, Nucl. Phys. **A505**, 267 (1989).
[7] O. Benhar, A. Fabrocini, S. Fantoni, and I. Sick, Nucl. Phys. **A579**, 493 (1994).
[8] D. Van Neck, A.E.L. Dieperink, and E. Moya de Guerra, Phys. Rev. C **51**, 1800 (1995).
[9] F. de Jong and R. Malfliet, Phys. Rev. C **44**, 998 (1991).
[10] P. Grangé, J. Cugnon, and A. Lejeune, Nucl. Phys. **A473**, 365 (1987).
[11] G. Röpke, L. Münchow, and H. Schulz, Nucl. Phys. **A379**, 536 (1982).
[12] H.S. Köhler, Nucl. Phys. **A529**, 209 (1991).
[13] M. Schmidt, G. Röpke, and H. Schulz, Ann. Phys. (N.Y.) **202**, 57 (1990).
[14] T. Alm, G. Röpke, A. Schnell, and H. Stein, Phys. Lett. B **346**, 233 (1995).
[15] T. Alm, B.L. Friman, G. Röpke, and H. Schulz, Nucl. Phys. **A551**, 45 (1993).
[16] H.F. Arellano, F.A. Brieva, and W.G. Love, Phys. Rev. C **50**, 2480 (1994).
[17] M. Baldo, I. Bombaci, and U. Lombardo, Phys. Lett. B **283**, 8 (1992).
[18] H. Stein, A. Schnell, T. Alm, and G. Röpke, Z. Phys. A **351**, 295 (1995).
[19] M. Baldo, U. Lombardo, and P. Schuck, Phys. Rev. C **52**, 975 (1995).
[20] D.J. Thouless, Ann. Phys. (N.Y.) **10**, 553 (1960).
[21] T. Alm, G. Röpke, and M. Schmidt, Phys. Rev. C **50**, 31 (1994).
[22] A.L. Fetter and J.D. Walecka, *Quantum Theory of Many-Particle Systems* (McGraw-Hill, New York, 1971).
[23] W.D. Kraeft, D. Kremp, W. Ebeling, and G. Röpke, *Quantum Statistics of Charged Particle Systems* (Plenum, New York, 1986).
[24] C. Bloch and C. De Dominicis, Nucl. Phys. **7**, 459 (1958); **10**, 181 (1959); **10**, 509 (1959).
[25] H.S. Köhler and R. Malfliet, Phys. Rev. C **48**, 1034 (1993).
[26] P. Danielewicz, Ann. Phys. (N.Y.) **197**, 154 (1990).
[27] H. S. Köhler and R. Malfliet, Acta Phys. Pol. B **24**, 513 (1993).
[28] W. Botermans and R. Malfliet, Phys. Rep. **198**, 115 (1990).
[29] J. Cugnon, P. Grangé, and A. Lejeune, J. Phys. (Paris) Colloq. **48**, C2-281 (1987).
[30] Y. Yamaguchi, Phys. Rev. **95**, 1628 (1954).
[31] T. R. Mongan, Phys. Rev. **178**, 1597 (1969).
[32] A. Ramos, A. Polls, and W.H. Dickhoff, Nucl. Phys. **A503**, 1 (1989).
[33] Kadanoff and G. Baym, *Quantum Statistical Mechanics* (Benjamin, New York, 1962).
[34] P. Ring and P. Schuck, *The Nuclear Many-Body Problem* (Springer, New York, 1980).
[35] T. Alm and P. Schuck (submitted to Phys. Rev. B).
[36] M. Baldo, I. Bombaci, G. Giansiracusa, U. Lombardo, C. Mahaux, and R. Sartor, Phys. Rev. C **41**, 1748 (1990).
[37] J.P. Blaizot and B.L. Friman, Nucl. Phys. **A372**, 69 (1981).
[38] L. Mathelitsch, W. Plessas, and W. Schweiger, Phys. Rev. C **26**, 65 (1982).
[39] N. Yamaguchi, S. Nagata, and T. Matsuda, Prog. Theor. Phys. **70**, 459 (1983).
[40] A. Lejeune, P. Grangé, M. Martzloff, and J. Cugnon, Nucl. Phys. **A453**, 189 (1986).
[41] V. Bernard and C. Mahaux, Phys. Rev. C **23**, 888 (1981).
[42] A. Ramos, W.H. Dickhoff, and A. Polls, Phys. Rev. C **43**, 2239 (1991).
[43] H.S. Köhler, Nucl. Phys. **A537**, 64 (1992).